Pergamon

Int. J. Heat Mass Transfer. Vol. 41, No. 12, pp. 1681–1692, 1998

Printed in Great Britain
0017–9310/98 $19.00 + 0.00

PII: S0017–9310(97)00303–7

Turbulent natural convection coupled with thermal radiation in large vertical channels with asymmetric heating

X. CHENG† and U. MÜLLER

Institute of Applied Thermo and Fluid Dynamics, Research Center Karlsruhe, Postfach 3640, D-76021 Karlsruhe, Germany

(*Received* 18 *December* 1996 *and in final form* 1 *September* 1997)

Abstract—Numerical and experimental investigations on turbulent natural air convection coupled with thermal radiation have been performed in a vertical rectangular channel with one-sided heated wall. A radiation model has been developed with two new features: an analytical method for computing the view factor and the macro-elements method for improving the numerical efficiency. Numerical studies have shown that the CFD code FLUTAN combined with the radiation model developed is an efficient and accurate numerical tool to investigate the flow and heat transfer behaviour in systems considered. It has shown that at intermediate and high wall emissivities thermal radiation contributes significantly to the total heat transfer by natural air convection, even at low temperatures of the heated wall. Based on the experimental and numerical results the following semi-empirical correlation has bene developed for describing the heat transfer of turbulent natural convection coupled with thermal radiation in a vertical, rectangular channel with one-sided heated wall:

$$Nu_t = 0.1 \cdot Ra^{1/3}\left\{1+(1+2\cdot l)\frac{0.919\cdot R_s}{1+0.513\cdot R_s}\right\}.$$

1. INTRODUCTION

Natural convection heat transfer in an open-ended vertical flow channel has been widely investigated in the past several decades owing to its important applications in electronic cooling, solar energy collectors and nuclear engineering [1–3]. The pioneering experimental work of Elenbass [4] laid the foundation for the study of natural convection in vertical channels of isothermal parallel plates. Analytical studies in this field go back to the numerical investigations of Bodoia and Osterle [5]. Both of the works were restricted to two-dimensional, laminar natural convection of air in vertical channel with symmetrical heatings. The effect of thermal radiation was excluded.

The flow and heat transfer behaviour in channels with asymmetrical heating was theoretically studied by Aung *et al.* [6, 7]. Boundary conditions of uniform wall temperature as well as uniform heat flux were considered. In addition, experimental investigations were performed in a small flow channel with uniform wall temperatures. The channel walls were made of materials of low emissivity, so that the effect of thermal radiation was excluded. The Rayleigh number realized in this experiment was less than 10^4. Experiments with higher Rayleigh number (up to 10^8) were conducted by Webb *et al.* [8]. The channel height is 15.2 cm. The ratio of the channel width to the channel depth is larger than six, so that the flow is considered to be two-dimensional. One of the plates was heated with uniform heat flux and the other is thermally insulated. The wall emissivity is kept low (approximately 0.1) to neglect the contribution of thermal radiation. More systematical investigations have been performed by Sparrow *et al.* [9, 10] into the laminar natural convection in open-ended channels under different boundary conditions and geometrical configurations. Based on experimental results, empirical heat transfer correlations have been derived, which agree well with the well known heat transfer correlation for the single-plate conditions.

The first numerical study concerning turbulent natural convection in an open-ended two-dimensional channel was performed by Borgers *et al.* [2]. The turbulent flow characteristics of air are predicted by a mixing length model. Based on numerical calculations empirical correlations were derived for induced flow rate and transferred heat rate, which are still not verified by experiments. Pica *et al.* [11] performed experimental investigations on turbulent natural convection of air in a large vertical channel with the channel height 2.6 m and the channel width 1.2 m. The channel depth was varied from 7.5–17 cm. One of the walls is heated with uniform heat flux, while the

† Author to whom correspondence should be addressed. Tel.: 49 7247 824897. Fax: 49 7247 824837. E-mail: xu.cheng@iatf.fzk.de.

NOMENCLATURE

A	surface area [m^{-2}]
B	channel width [m]
C_p	specific heat [J (kg K)$^{-1}$]
e	emitted heat flux defined as $\sigma \cdot \varepsilon \cdot T^4$ [W m^{-2}]
E	emitted heat power [W]
g	gravitational acceleration [m s^{-2}]
h	heat transfer coefficient [W (m^2 K)$^{-1}$]
H	channel height [m]
k	kinetic energy of turbulence [m^2 s^{-2}]
l	aspect ratio, defined as L/B
l_0	equivalent hydraulic diameter of the flow channel [m]
L	channel depth [m]
Nu	Nusselt-number
O	outgoing heat power [W]
P	pressure [Pa]
Pr	Prandtl-number
q	heat flux [W m^{-2}]
Q	heat power [W]
Ra	Rayleigh-number, defined in equation (24)
R_s	parameter defined in equation (18)
St	Stefan-number, defined in equation (A.21)
T	temperature [°C]
u	velocity [m s^{-1}]
X, Y, Z	coordinates [m].

Greek symbols

β	thermal expansion coefficient [1 K]
λ	thermal conductivity [W (m K)$^{-1}$]
ε	emissivity or dissipation rate of kinetic energy k [m^2 s^{-3}]
μ	dynamic viscosity [kg (m s)$^{-1}$]
ν	kinematic viscosity [m^2 s^{-1}]
ρ	density [kg m^{-3}]
τ	shear stress [N m^{-2}]
φ	view factor.

Subscripts

c	convection
f	fluid
in	inlet cross-section
r	radiation
t	total
w	wall
1	heated wall
2	unheated wall.

other walls are made of glass plates and kept adiabatic. Because of the low emissivity of the glass plates the effect of thermal radiation was neglected. Based on experimental results, empirical correlations for induced flow and heat transfer were derived.

In many technical systems with natural air convection and with asymmetrical heating the effect of thermal radiation has to be taken into account. Combined natural convection and thermal radiation heat transfer between vertical flat plates was first of all numerically investigated by Carpenter *et al.* [12]. It was found that at high Rayleigh number thermal radiation reduces significantly the heated wall temperature by keeping heat flux uniform and constant. Similar numerical studies were conducted by Moutsoplou *et al.* [13]. All these works have been restricted to two-dimensional laminar flow conditions.

The above critical bibliographic survey underlines the deficiency in experimental as well as in theoretical studies on turbulent natural convection heat transfer coupled with thermal radiation in a three-dimensional vertical channel with asymmetrical heating. This kind of problem, however, has recently drawn considerable attention due to its application in nuclear engineering. In the present study theoretical and experimental analysis has been performed for a better understanding and for looking inside of the flow and heat transfer behaviour in the system considered.

2. NUMERICAL SIMULATION

Numerical simulation of 3-D turbulent natural convection coupled with thermal radiation requires high capabilities of a computer code. In the present study the CFD code FLUTAN is used which is developed at the Research Center Karlsruhe [14].

2.1. *Basic equations*

The channel geometry considered is a rectangular, vertical channel, as indicated in Fig. 1. One of the walls ($Y = L$) is heated and kept at a constant temperature T_1. All the walls are thermally insulated against the ambient surroundings. The heat conduction inside the walls is neglected. The air entering the flow channel has a uniform temperature distribution T_{in}. The basic equations for the turbulent flow under stationary conditions are summarized as follows:

Mass conservation

$$\frac{\partial(\rho u_i)}{\partial x_i} = 0. \tag{1}$$

Momentum conservation

$$\frac{\partial(\rho u_i u_j)}{\partial x_j} = -\frac{\partial P}{\partial x_i} + \frac{\partial}{\partial x_i}\left[(\mu + \mu_t)\frac{\partial u_i}{\partial x_i} - \frac{2}{3}\rho k\right] + \rho g_i. \tag{2}$$

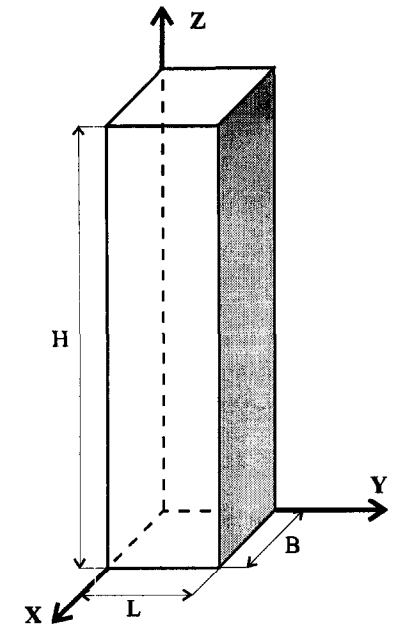

Fig. 1. Flow channel and coordinate system.

Energy conservation

$$\frac{\partial(\rho u_j T)}{\partial x_j} = \frac{\partial}{\partial x_i}\left[\left(\frac{\mu}{Pr} + \frac{\mu_t}{\sigma_t}\right)\frac{\partial T}{\partial x_i}\right]. \tag{3}$$

Transport equation of the kinetic energy of turbulence k

$$\frac{\partial(\rho u_j k)}{\partial x_j} = P_k + G_k - \rho\varepsilon + \frac{\partial}{\partial x_j}\left[\left(\frac{\mu+\mu_t}{\sigma_k}\right)\frac{\partial k}{\partial x_j}\right]. \tag{4}$$

Transport equation of the dissipation rate of the kinetic energy ε

$$\frac{\partial(\rho u_j \varepsilon)}{\partial x_j} = C_1\frac{\varepsilon}{k}(P_k + G_k)\left(1 - C_3\frac{G_k}{P_k}\right) - C_2\frac{\rho\varepsilon^2}{k} + \frac{\partial}{\partial x_j}\left[\left(\frac{\mu+\mu_t}{\sigma_\varepsilon}\right)\frac{\partial \varepsilon}{\partial x_j}\right] \tag{5}$$

with

$$\mu_t = \frac{C_\mu \rho k^2}{\varepsilon} \tag{6}$$

$$P_k = \mu_t\left[\frac{\partial u_i}{\partial x_j}\left(\frac{\partial u_i}{\partial x_j} + \frac{\partial u_j}{\partial x_i}\right)\right] \tag{7}$$

$$G_k = -\frac{\mu_t}{\rho\sigma_t}\frac{\partial \rho}{\partial T}\left(\frac{\partial T}{\partial x_j}g_j\right). \tag{8}$$

In the immediate vicinity of a solid wall where large variation in the values of turbulent properties exists, the so-called wall-function treatment is applied to compute wall shear stress

Table 1. Constants in the basic equations

C_μ	C_1	C_2	C_3	σ_k	σ_ε	σ_t	κ	E
0.09	1.44	1.92	0.8	1.0	1.3	0.9	0.4	9.0

$$\tau_w = \frac{\kappa\rho k^{1/2} u C_\mu^{1/4}}{\ln(EyC_\mu^{1/4}k^{1/2}/\nu)} \tag{9}$$

and convective heat flux

$$q_c = \frac{\kappa\rho k^{1/2} C_\mu^{1/4} C_P (T_w - T)}{\ln(EyC_\mu^{1/4}k^{1/2}/\nu) + 9.24\kappa(Pr/\sigma_t - 1)(\sigma_t/Pr)^{1/4}}. \tag{10}$$

Here y is the distance from the wall. The constants in the basic equations above are summarized in Table 1.

2.2. *Thermal radiation model*

The convective heat transfer is coupled with thermal radiation by the thermal boundary condition at unheated walls, where the net radiative heat must be transferred by natural convection of air:

$$q_r = q_c, \quad \text{at } X = 0 \quad \text{or} \quad X = B \quad \text{or} \quad Y = 0. \tag{11}$$

The convective heat flux q_c is determined by equation (10). To calculate the net radiative heat flux q_r, a thermal radiation model with high numerical efficiency has been developed. In this model the fluid (air) is considered radiatively non-participating and the walls are grey and diffuse. The net radiative heat power of a surface element $Q_{r,i}$ is computed by the net-radiation method for enclosures [15]:

$$\left(\frac{Q_{r,i}}{\varepsilon_i}\right) = \left(\frac{E_i}{\varepsilon_i}\right) - \sum_j \left(\frac{E_j}{\varepsilon_j}\right)\varphi_{j,i} + \sum_j (1-\varepsilon_j)\varphi_{j,i}\left(\frac{Q_{r,j}}{\varepsilon_j}\right). \tag{12}$$

The above radiation equation can be solved either directly or iteratively. The direct solution is exact and usually needs larger computing expenditure. An iterative solution, e.g. the Gauß–Seidel iteration, requires only a few iterations for intermediate or high wall emissivities. Nevertheless, at low emissivities the direct solution method is more efficient than the iterative method.

The radiative heat power can be easily computed by solving equation (12), as long as the view factors φ_{ij} are known. Generally, view factor can only be obtained numerically. For a flow channel in the Cartesian coordinate system where boundary walls are either parallel or perpendicular to each other, the view factor between any two surface elements has been derived analytically. Figure 2 shows two different cases: (a) two parallel surface elements and (b) two perpendicular surface elements. To specify the dimen-

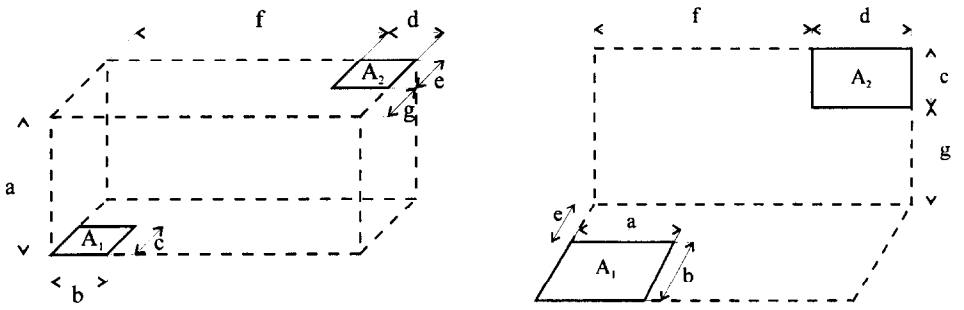

(a) two parallel surface elements *(b) two perpendicular surface elements*

Fig. 2. Geometric parameters of two surface elements in a Cartesian coordinate system.

sions of any two surface elements and their relative positions, seven geometric parameters are needed, indicated as a, b, c, d, e, f, g in Fig. 2. The view factor for two parallel surface elements (Fig. 2(a)) is derived as the following:

$$\frac{\varphi_{12}\cdot\pi\cdot A_1}{a^2} = \sum_{i=1}^{4} Z_i \sum_{j=1}^{4} S_j \cdot \left\{\frac{1}{2}\cdot X_j \cdot \sqrt{1+Y_i^2}\cdot \arctan\left(\frac{X_j}{\sqrt{1+Y_i^2}}\right)\right\} + \sum_{i=1}^{4} Z_i \sum_{j=1}^{4} S_j \cdot \left\{\frac{1}{2}\cdot Y_i \cdot \sqrt{1+X_j^2}\cdot \arctan\left(\frac{Y_i}{\sqrt{1+X_j^2}}\right)\right\} - \sum_{i=1}^{4} Z_i \sum_{j=1}^{4} S_j \cdot \left\{\frac{1}{4}\cdot \ln(1+X_j^2+Y_i^2)\right\}. \quad (13)$$

For two perpendicular surface elements (Fig. 2(b)) the view factor can be calculated by:

$$\frac{\varphi_{12}\cdot\pi\cdot A_1}{a^2} = \sum_{i=1}^{4} Z_i \sum_{j=1}^{4} S_j \cdot \left\{\frac{1}{8}\cdot (X_i^2 - Y_j)\cdot \ln(X_i^2+Y_j)\right\} + \sum_{i=1}^{4} Z_i \sum_{j=1}^{4} S_j \cdot \left\{\frac{1}{2}\cdot \sqrt{Y_j}\cdot X_i \arctan\left(\frac{X_i}{\sqrt{Y_j}}\right)\right\}. \quad (14)$$

The parameters X_i, Y_i, Z_i and S_i in equation (13) and in equation (14) are summarized in Table 2 and Table 3, respectively.

For computing flow conditions accurately, the computational domain has to be divided into sufficiently small sub-zones. The fine discretization results in a large number of surface elements. If the radiation equation, equation (12), is applied to all the surface elements, a large storage capacity and a huge computing time are needed. Therefore, the so-called *macro-elements method* has been developed in this study, to improve the numerical efficiency.

Table 2. Parameters in equation (12)

	X_i	Y_i	Z_i	S_i
$i=1$	$(f+d)/a$	$(g+e)/a$	$+1$	$+1$
$i=2$	$(b-f)/a$	g/a	-1	$+1$
$i=3$	$(b-f-d)/a$	$(c-g-e)/a$	-1	-1
$i=4$	(f/a)	$(c-g)/a$	$+1$	-1

Table 3. Parameters in equation (13)

	X_i	Y_i	Z_i	S_i
$i=1$	$(f+d)/a$	$[g^2+(e+b)^2]/a^2$	$+1$	$+1$
$i=2$	$(a-f)/a$	$[e^2+(g+c)^2]/a^2$	$+1$	$+1$
$i=3$	$(a-f-d)/a$	$[g^2+e^2])/a^2$	-1	-1
$i=4$	(f/a)	$[(g+c)^2+(e+b)^2]/a^2$	-1	-1

The basic idea of the macro-elements method is to combine a few surface elements (micro-elements) to form *one* macro-element. The emissivity of all the surface elements which belong to the same macro-element is identical. The effective surface temperature of a macro-element is computed by the following equation:

$$T_I^4 = \frac{1}{A_I}\left[\sum_{i\in I} A_i \cdot T_i^4\right]. \quad (15)$$

The subscripts 'i' and 'I' stand for micro-elements and macro-elements, respectively. After solving the radiation equation for the macro-elements, the net radiative heat flux of a micro-element can be determined by:

$$q_{r,i} = q_{r,I} + e_i - e_I. \quad (16)$$

Numerical analysis shows that by a suitable selection of the macro-elements the additional error resulted by introducing the macro-elements method can be kept negligibly small, whereas the storage needs and the computing time can be reduced significantly.

3. NUMERICAL RESULTS AND DISCUSSIONS

For the results presented in this paper the inlet air temperature T_{in} is 20.0°C, the channel width B is 0.5

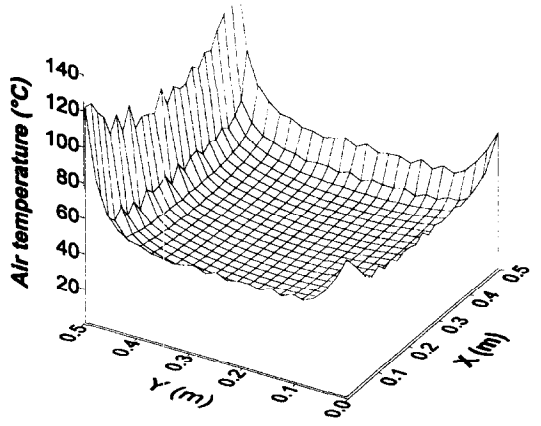

(a)

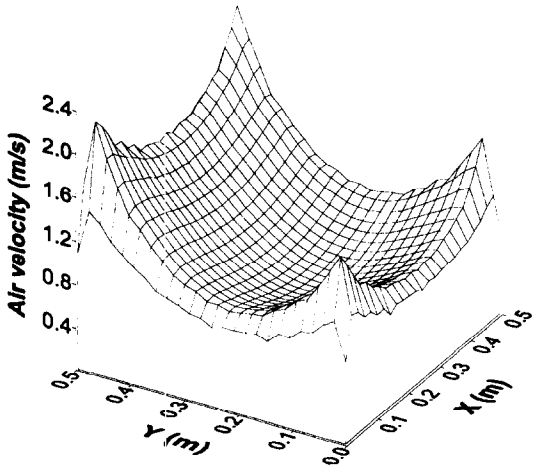

(b)

Fig. 3. Profiles of the air temperature (a) and air velocity (b). $T_1 = 150°C$, $\varepsilon = 0.9$, $L = 0.5$ m.

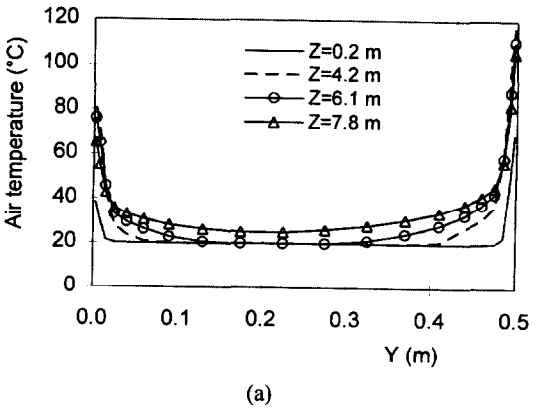

(a)

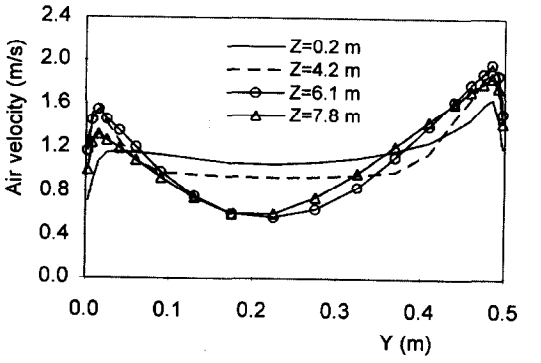

(b)

Fig. 4. Air temperature (a) and air velocity (b) along the middle line ($X = 0.25$ m). $T_1 = 150°C$, $\varepsilon = 0.9$, $L = 0.5$ m.

m and the channel height H is 8.0 m. Figure 3 illustrates the calculated profiles of the air temperature and the air velocity at the channel outlet cross-section for the following *reference* condition : heated wall temperature (T_1) 150°C, wall emissivity (ε) 0.9 and channel depth (L) 0.5 m. It can be seen that the air temperature decreases rapidly with the distance from the heated wall. The maximum temperature locates in the corner where the heated wall connects the side wall. Due to thermal radiation the air temperature increases again by approaching the side wall and the back wall. The minimum value of the air temperature appears in the central region. Similar results have also been obtained for the air velocity distribution (Fig. 3(b)). As expected for natural convection, the maximum air velocity is observed close to the wall surface. Again, due to thermal radiation a minimum of the air velocity is found in the central region.

Figure 4 shows the air temperature and the air velocity along the mid-line ($X = 0.25$ m) vs. the distance from the back wall (Y) at different axial levels. Near the inlet cross-section ($Z = 0.2$ m) the air temperature distribution is uniform (20°C) over the entire channel depth except for near the walls. At higher axial levels the temperature near the walls increases and the region affected by the higher wall temperature enlarges. Near the outlet cross-section this affected region spreads over the entire cross section, so that the air temperature in the central region is clearly higher than the inlet air temperature (20°C). The air velocity has a well uniform distribution in the central region in the lower part of the channel. At higher axial levels the air velocity near the walls increases, whereas it decreases in the central region.

Figure 5 shows the air temperature and air velocity at the outlet cross-section along the midline ($X = 0.25$ m) vs. the distance from the back wall at different values of the channel depth and the wall emissivity. By decreasing the wall emissivity from 0.9 down to 0.4 the effect of thermal radiation and, consequently, the temperature on the back wall reduces. This leads to a reduction in the air temperature as well as in the air velocity near the back wall. In the region far away from the back wall the flow condition remains nearly

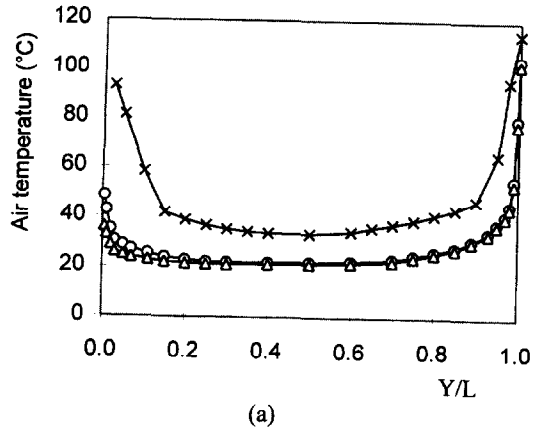

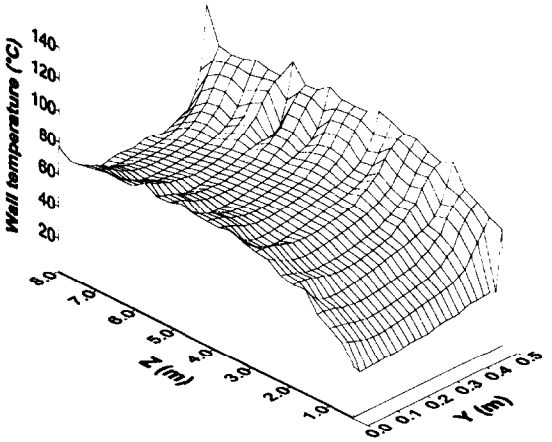

Fig. 6. Temperature distribution on the side wall. $T_1 = 150°C$, $\varepsilon = 0.9$, $L = 0.5$ m.

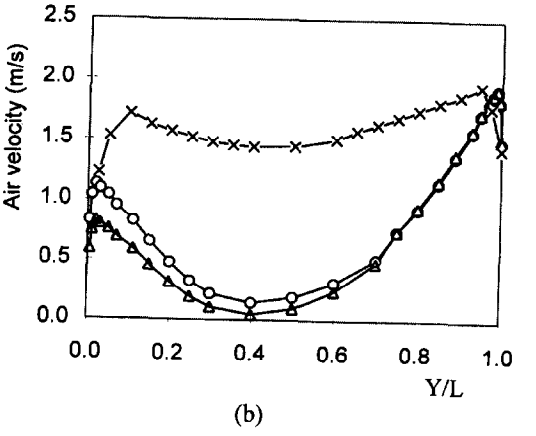

Fig. 5. Air temperature (a) and air velocity (b) at the outlet cross-section and $X = 0.25$ m. ○: $T_1 = 150°C$, $\varepsilon = 0.9$, $L = 1.0$ m; △: $T_1 = 150°C$, $\varepsilon = 0.4$, $L = 1.0$ m; x: $T_1 = 150°C$, $\varepsilon = 0.9$, $L = 0.2$ m.

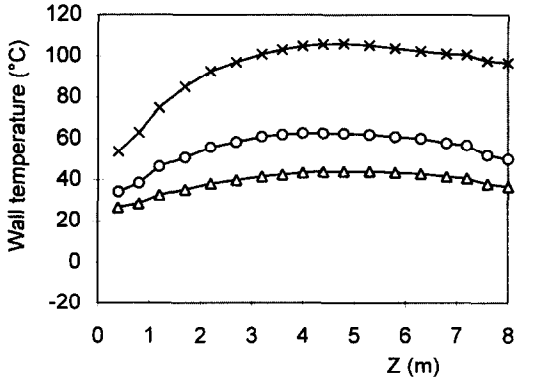

Fig. 7. Temperature distribution on the back wall along the middle line ($X = 0.25$ m). ○: $T_1 = 150°C$, $\varepsilon = 0.9$, $L = 1.0$ m; △: $T_1 = 150°C$, $\varepsilon = 0.4$, $L = 1.0$ m; x: $T_1 = 150°C$, $\varepsilon = 0.9$, $L = 0.2$ m.

unchanged. Reducing the channel depth enhances the radiative heat exchange between the heated wall and the back wall, so that the temperature on the back wall increases. This leads to a higher air temperature and higher air velocity.

Figure 6 shows the temperature distribution on the side wall for the reference condition. The temperature on the side wall decreases rapidly with the distance from the heated wall. It increases again towards the back wall due to higher air temperature in the corner region (see Fig. 3). With increasing axial level the wall temperature at first increases and then decreases again towards the channel outlet cross-section due to radiative heat loss to the environment.

Figure 7 shows the temperature on the back wall along the mid-line ($X = 0.25$ m) vs. the axial location (Z) for different values of the channel depth and the wall emissivity. Reducing the wall emissivity from 0.9–0.4 results in a reduction in the wall temperature of about 20°C. A reduction of the channel depth from 1.0–0.2 m leads to an increase in the wall temperature of about 40°C. The maximum temperature locates at the elevation $Z \approx 5.0$ m.

Figure 8 presents the profiles of the convective heat flux and the radiative heat flux at the heated wall. Due to the development of the boundary layer the convective heat flux in the inlet region is much higher than in the other regions, where the convective heat flux remains nearly uniform. Again, due to the radiative heat loss to the ambient surroundings the radiative heat flux in the inlet as well as in the outlet region is higher than in the middle region where the radiative heat flux has a well uniform distribution.

By dividing the total channel height into three zones, i.e. the inlet zone ($Z \leqslant 2.0$ m), the middle zone (2.0 m $\leqslant Z \leqslant 6.0$ m) and the outlet zone ($Z \geqslant 6.0$ m), the average heat flux on the heated wall in each zone is shown in Fig. 9. The average heat flux in the inlet zone is about 40 and 25% higher than that in the middle zone and in the outlet zone, respectively. It is also clearly seen that for the condition considered the heat power transferred from the heated wall by

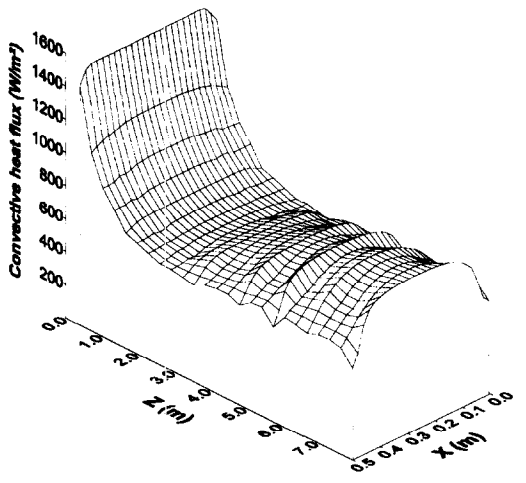

(a)

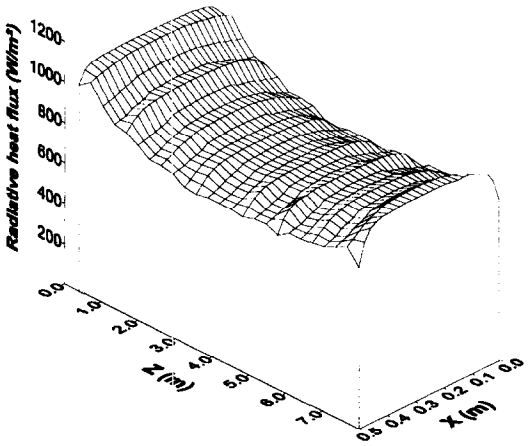

(b)

Fig. 8. Profiles of the convective (a) and radiative heat flux (b) on the heated wall. $T_1 = 150°C$, $\varepsilon = 0.9$, $L = 0.5$ m.

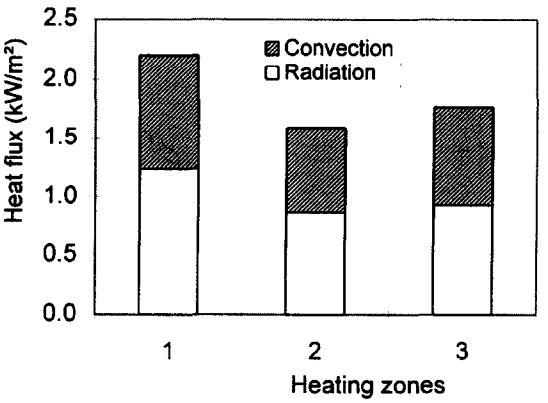

Fig. 9. Average heat flux on the heated wall in different zones. $T_1 = 150°C$, $\varepsilon = 0.9$, $L = 0.5$ m.

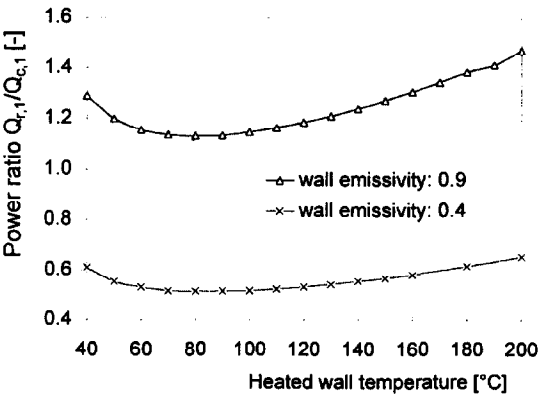

Fig. 10. Power ratio vs. the heated wall temperature. $T_1 = 150°C$, $L = 0.5$ m.

radiation is comparable to that transferred directly by natural convection.

Figure 10 shows the ratio of the heat power transferred from the heated wall by thermal radiation to the heat power transferred directly by convection vs. the heated wall temperature for two different values of wall emissivity. At high wall emissivity ($\varepsilon = 0.9$) the power ratio is larger than one. In this case more heat is transferred from the heated wall by thermal radiation than by convection. The minimum value of the ratio is found by a heated wall temperature of about 80°C. At low wall emissivity ($\varepsilon = 0.4$) the ratio of the radiative heat power to the convective heat power is still larger than 50%. The minimum of the ratio is also found by a heated wall temperature of about 80°C. This emphasizes the strong effect of thermal radiation on the overall heat transfer even at low values of wall emissivity and at low wall temperatures. This minimum phenomenon in the power ratio will be explained in the next paragraph.

Figure 11 illustrates the air mass flow rate and the transferred heat power vs. the heated wall temperature at different values of the channel depth and the wall emissivity. By increasing the heated wall temperature the air mass flow rate as well as the heat power increases. The heat power increases about 200% by increasing the heated wall temperature from 100–200°C, whereas the air mass flow rate increases only about 50%. By reducing the channel depth from 1.0–0.5 m the air mass flow rate decreases about 40%, whereas the heated power remains nearly unchanged. Reducing the wall emissivity from 0.9–0.4 results in a reduction in the air mass flow rate and the heat power of approximately 20 and 30%, respectively.

4. COMPARISON WITH EXPERIMENTAL DATA

In addition to the numerical investigation experiments have been performed using a vertical rec-

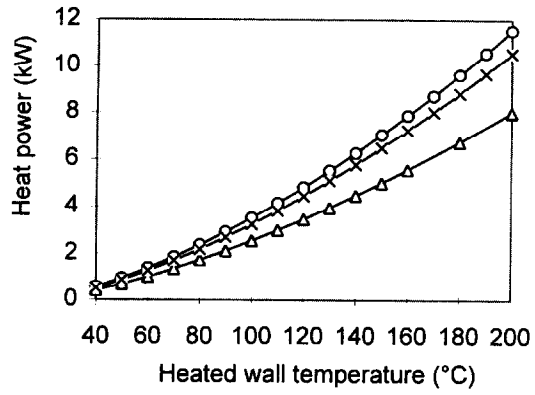

(a) Heat power

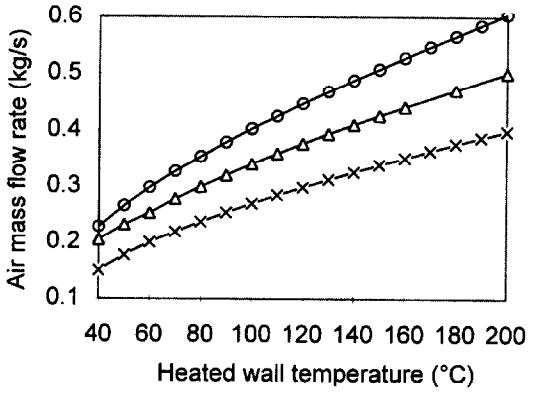

(b) Air mass flow rate

Fig. 11. Transferred heat power and air mass flow rate vs. the heated wall temperature. ○: $\varepsilon = 0.9$, $L = 1.0$ m; △: $\varepsilon = 0.4$, $L = 1.0$ m; x: $\varepsilon = 0.9$, $L = 0.5$ m.

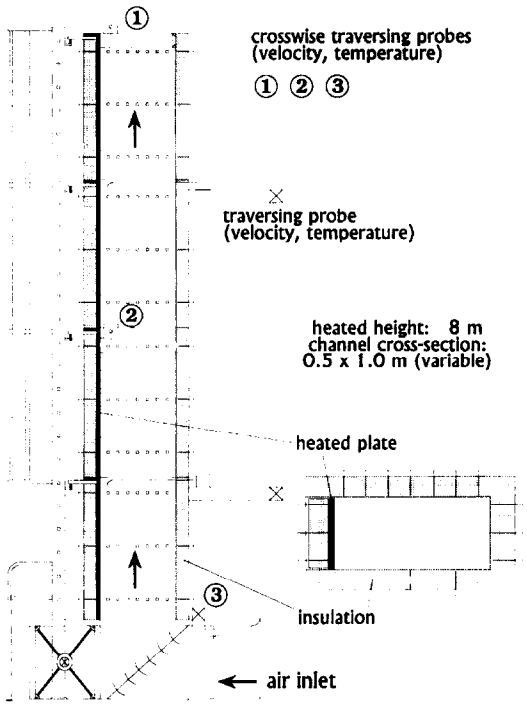

Fig. 12. Schematical diagram of the test channel.

Table 4. Measurement accuracy

Temperature	Air velocity	Pressure	Heating power
±0.75°C	±2.0%	±0.5%	±1.0%

tangular channel of which one wall is electrically heated, as shown in Fig. 12. The unheated walls are made of thin steel plates, so that the effect of heat conduction inside the walls is negligible. All the walls are thermally insulated from the ambient surroundings. The channel width, i.e. the width of the heated wall, is 0.5 m. The channel depth, i.e. the distance from the heated wall to the back wall, can be changed up to 1.0 m, so that the effect of the channel geometry on heat transfer will be studied. The heated wall has a total height of 8.0 m and consists of four individually heatable plates. The heating power of each heated plate is separately controlled, to achieve a uniform distribution of the heated wall temperature. The heated wall temperature ranges from 100–175°C. Two different values of wall emissivity (0.4, 0.9) are realized to investigate its influence on the total heat transfer. The test facility is equipped among others with approximately 170 thermocouples to measure the distribution of wall temperatures. Traversing probes for recording the air temperature and the air velocity distributions are installed at five different elevations with thermocouples for the temperature measurement and with Prandtl-tubes for the velocity measurement. Moreover, the average ambient temperature, the pressure at the channel inlet, the air humidity and the heating powers of each heated plate are recorded. The accuracy of different measurement parameters is summarized in Table 4. Detailed descriptions of the test facility, measurement techniques and some experimental results can be found in the previous publications [16].

Figure 13 compares the calculated heat power transferred from the heated wall with the experimental results. An excellent agreement between the numerical and the experimental results has been found. For all test points considered the deviation between the experimental data and the numerical results is less than 10%.

Figure 14 compares the calculated air temperature and air velocity at the channel outlet cross-section along the middle line ($X = 0.25$ m) with experimental data for the reference condition. Again, the CFD code FLUTAN combined with the radiation model developed reproduces the experimental results accurately and is proven to be successfully verified for

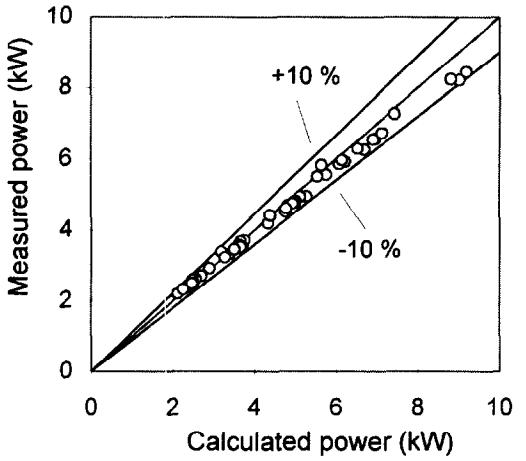

Fig. 13. Comparison of the calculated heat powers with the measured data.

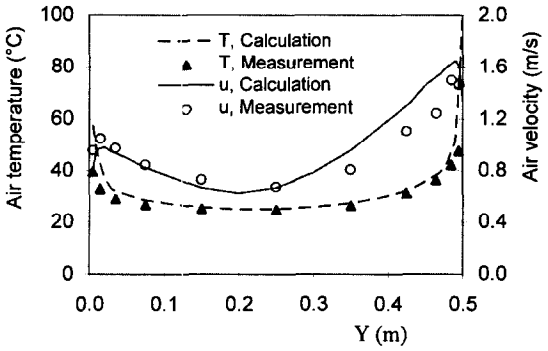

Fig. 14. Comparison of the calculated air temperature and air velocity with the test data. $T_1 = 150°C$, $\varepsilon = 0.9$, $L = 0.5$ m, $X = 0.25$ m, $Z = 7.8$ m.

turbulent natural convection coupled with thermal radiation in a vertical, rectangular channel with asymmetric heating.

5. HEAT TRANSFER RELATIONSHIP

A bibliographic survey has emphasised the deficiency in correlations describing the heat transfer of turbulent natural convection coupled with thermal radiation in a vertical, rectangular channel with asymmetric heating. Therefore, efforts have been made in the present work to develop a semi-empirical correlation. The total heat flux on the heated wall consists of two parts, i.e. the convective heat flux and the radiative heat flux. The ratio of both heat fluxes can be expressed as the following (see Appendix):

$$\frac{q_{r,1}}{q_{c,1}} = (1+2l)\frac{aR_s}{1+bR_s} \tag{17}$$

with

$$R_s = \frac{1}{2+2l-\varepsilon}\frac{St}{Nu_c}. \tag{18}$$

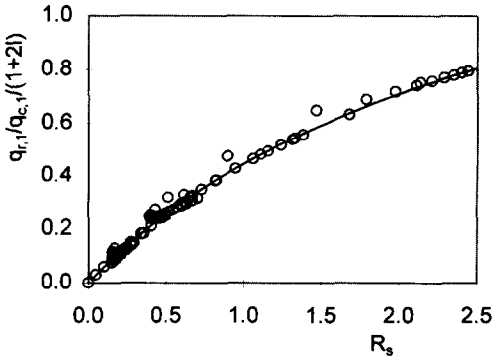

Fig. 15. Relationship between the heat flux ratio and the parameter R_s.

To determine the coefficients a and b in equation (17), numerical calculations have been performed with different parameters: heated wall temperature (30–200°C), wall emissivity (0.0–1.0), channel depth (0.1–1.0 m) and channel width (0.1–1.0 m). The channel height is 8.0 m. Only the results in the middle zone ($2.0\ \text{m} \leqslant Z \leqslant 6.0$ m) are used for computing the power ratio and the parameter R_s, so that the effect appearing in the inlet zone and in the outlet zone can be excluded. Figure 15 presents the numerical results. It can be clearly seen that for all conditions considered the relationship between $(q_{r,1}/q_{c,1})[1/(1+2l)]$ and R_s can be well correlated by a single curve. By using the minimum error square principle both the coefficients a and b are determined:

$$a = 0.919$$

$$b = 0.513.$$

It yields

$$\frac{q_{r,1}}{q_{c,1}} = (1+2l)\frac{0.919R_s}{1+0.513R_s}. \tag{19}$$

The total Nusselt-number is defined as

$$Nu_t = Nu_c\left\{1+\frac{q_{r,1}}{q_{c,1}}\right\} = Nu_c\left\{1+(1+2l)\frac{0.919R_s}{1+0.513R_s}\right\}. \tag{20}$$

The convective Nusselt-number Nu_c can be derived by using experimental data obtained under the following test conditions: heated wall temperature 100–175°C, channel depth 0.25–1.0 m, wall emissivity 0.4–0.9. The total Nusselt-number Nu_t and the parameter R_s can be directly determined from the experimental data. The convective Nusselt-number Nu_c is then calculated according to equation (20). Figure 16 shows the convective Nusselt-number in dependence on the Rayleigh-number, which is directly determined from the experimental data. It can be seen that the data points can be well correlated by the following equation:

$$Nu_c = 0.1 \cdot Ra^{1/3}. \tag{21}$$

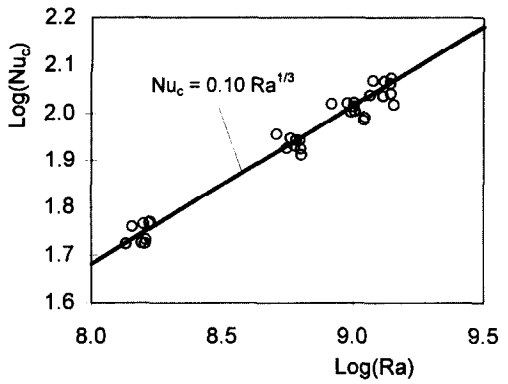

Fig. 16. Relationship between the convective Nusselt-number and the Rayleigh-number.

This equation agrees well with some well known heat transfer correlations for turbulent natural convection on a single infinite vertical plate [17]. The final correlation derived is:

$$Nu_t = 0.1 \cdot Ra^{1/3} \left\{ 1 + (1+2l) \frac{0.919 R_s}{1+0.513 R_s} \right\} \quad (22)$$

with

$$R_s = \frac{1}{2+2l-\varepsilon} \cdot \frac{St}{0.1 \cdot Ra^{1/3}} \quad (23)$$

$$Ra = \frac{\beta \cdot C_p \cdot \rho \cdot g \cdot (T_1 - T) \cdot l_0^3}{\nu \cdot \lambda}. \quad (24)$$

The parameter ranges based on which the semi-empirical correlation has been developed are identified as following:

Rayleigh-number Ra	10^7–$2 \cdot 10^9$
Stefan-number St	0–$6 \cdot 10^2$
Aspect ratio l	0.1–10.0
Heated wall temperature T_1	20–200°C

With the help of the heat transfer correlation developed the minimum phenomenon in the power ratio (see Fig. 10) can be easily explained. According to equation (19) and equation (23) the ratio of the radiative to the convective heat flux is written as:

$$\frac{q_{r,1}}{q_{c,1}} \propto \frac{T_1^3 (T_1 - T_f)^{-1/3}}{1 + c \cdot T_1^3 (T_1 - T_f)^{-1/3}} \quad (25)$$

with

$$c = \frac{5.13}{2+2l-\varepsilon} \cdot \frac{4 \cdot \sigma \cdot \varepsilon \cdot l_0}{\lambda} \cdot \left(\frac{\beta \cdot C_p \cdot \rho \cdot g \cdot l_0^3}{\nu \cdot \lambda} \right)^{-1/3}. \quad (26)$$

The minimum value of the power ratio appears by a heated wall temperature of:

$$T_1 = \tfrac{9}{8} T_f.$$

Here T_1 and T_f are in Kelvin. For an average air temperature of 20°C, the minimum power ratio locates at a heated wall temperature of about 60°C.

6. CONCLUSIONS

Although natural convection heat transfer in an open-ended vertical flow channel has been widely investigated in the past several decades, a thorough bibliographic survey underlines the deficiency in experimental as well as in theoretical studies on turbulent natural convection heat transfer coupled with thermal radiation in a three-dimensional vertical channel with asymmetrical heating. This kind of problem, however, has recently drawn considerable attention due to its application in nuclear engineering. In the present study theoretical and experimental analysis has been performed for a better understanding and for looking inside of the flow and heat transfer behaviour in a vertical rectangular channel with one-sided heated wall. The effect of the heated wall temperature, the wall emissivity and the channel geometry on the flow and heat transfer behaviour has been studied. A broad and detailed data base has been generated for the validation of computer codes and for development of physical models. The following specific main conclusions can be drawn:

- A radiation model with high numerical efficiency has been developed. Analytical equations have been derived for calculating the view factor between any two surface elements. The so-called macro-elements method has been developed which improves the numerical efficiency significantly.
- The CFD code FLUTAN combined with the radiation model developed has been proven to be an accurate and efficient numerical tool to investigate the flow and heat transfer behaviour of turbulent natural air convection coupled with thermal radiation in a vertical, rectangular channel with asymmetric heating.
- At intermediate and high wall emissivities thermal radiation contributes significantly to the total heat transfer by natural air convection, even at low temperatures of the heated wall. The ratio of the radiative to the convective heat power shows its minimum at a heated wall temperature of about 80°C.
- In the region near the channel inlet cross-section the convective heat transfer is much stronger than in other regions. This entrance effect diminishes rapidly with the distance from the entrance and vanishes at a distance larger than 2 m. Due to the radiative heat loss to the environment the radiative heat flux shows an increase towards the inlet and the outlet cross-section and has its minimum near the middle elevation.
- The convective heat transfer on the heated wall can be well described by a conventional correlation valid for turbulent natural convection on a infinite vertical plate.
- Based on the experimental and numerical results

the following semi-empirical correlation has been developed for describing the heat transfer of turbulent natural convection coupled with thermal radiation in a vertical, rectangular channel with one-sided heated wall:

$$Nu_t = 0.1 \cdot Ra^{1/3} \cdot \left\{1 + (1+2 \cdot l)\frac{0.919 \cdot R_s}{1+0.513 \cdot R_s}\right\}.$$

Acknowledgement—This work is partially supported by the 'Bundesministerium für Bildung, Wissenschaft, Forschung und Technologie' under the Project Grant 15NU 0961.

REFERENCES

1. Peterson, G. P. and Ortega, A., Thermal control of electronic equipment and devices. *Advances Heat Transfer*, 1990, **20**, 281–310.
2. Borgers, T. R. and Akbari, H., Free convection turbulent flow within the trombe wall channel. *Solar Energy*, **33**(3/4), 253–264.
3. Nishi, Y. and Kinoshita, I., Study on reactor vessel auxiliary cooling system with high-performance heat collector. *Proceedings of the International Conference on Fast Reactors and Related Fuel Cycles*. Kyoto, Japan, October 1995, pp. 12.6-1–12.6-9.
4. Elenbass, W., Heat dissipation of parallel plates by free convection. *Physica*, 1942, **9**, 1–28.
5. Bodoia, J. R. and Osterle, J. F., The development of free convection between heated vertical plates. *Journal of Heat Transfer*, 1962, 40–44.
6. Aung, W., Fully developed laminar free convection between vertical plates heated asymmetrically. *International Journal of Heat and Mass Transfer*, 1972, **15**, 1577–1580.
7. Aung, W., Fletcher, L. S. and Sernas, V., Developing laminar free convection between vertical flat plates with asymmetric heating. *International Journal of Heat and Mass Transfer*, 1972, **15**, 2293–2308.
8. Webb, B. W. and Hill, D. P., High Rayleigh number laminar natural convection in an asymmetrically heated vertical channel. *Journal of Heat Transfer*, 1989, **111**, 649–656.
9. Sparrow, E. M., Shah, S. and Prakash, C., Natural convection in a vertical channel: I. Interacting convection and radiation. II. The vertical plate with and without shrouding. *Numerical Heat Transfer*, 1980, **3**, 297–314.
10. Sparrow, E. M., Chrysler, G. M. and Azevedo, L. F., Observed flow reversals and measured-predicted Nusselt numbers for natural convection in a one-sided heated vertical channel. *Journal of Heat Transfer*, 1984, **106**, 325–332.
11. La Pica, A., Rodono, G. and Volpes, R., An experimental investigation on natural convection of air in a vertical channel. *International Journal of Heat and Mass Transfer*, 1993, **36**(3), 611–616.
12. Carpenter, J. R., Briggs, D. G. and Sernas, V., Combined radiation and developing laminar free convection between vertical flat plates with asymmetric heating. *Journal of Heat Transfer*, 1976, 95–100.
13. Moutsoglou, A. and Wong, Y. H., Convection–radiation interaction in buoyancy-induced channel flow. *Journal of Thermophysics*, 1989, **3**(2), 175–181.
14. Grötzbach, G. and Cheng, X., Development progress of the FLUTAN code for modelling heat transfer in LWR-systems (in German). *Proceedings of the Annual Meeting on Nuclear Technology '96*, Mannheim, May 1996, pp. 168–171.
15. Siegel, R. and Howell, J. R., *Thermal Radiation Heat Transfer*, 3rd edn. Hemisphere, Washington, 1992.
16. Cheng, X., Erbacher, F. J. and Neitzel, H. J., Passive containment cooling for next generation water cooled reactors. *Proceedings of the ICONE-4 Conference*, 1996, pp. 343–356.
17. Churchill, S. W. and Chu, H. H. S., Correlating equations for laminar and turbulent free convection from a vertical plate. *International Journal of Heat and Mass Transfer*, 1975, **18**, 1323–1329.

APPENDIX: RATIO OF THE RADIATIVE HEAT FLUX TO THE CONVECTIVE HEAT FLUX

In the flow channel, indicated in Fig. 1, heat is transferred from the heated wall by both thermal radiation and convection. The total heat flux on the heated wall consists of the convective heat flux and the radiative heat flux:

$$q_t = q_c + q_r = q_c\left(1 + \frac{q_r}{q_c}\right). \tag{A.1}$$

To derive the ratio of the radiative heat flux to the convective heat flux, the following assumptions are made:

- The heated wall has a uniform temperature distribution T_1, and the temperature on all the unheated walls is also uniform T_2.
- The channel height is much larger than both the channel width and the channel depth, so that the entrance effect on total heat transfer as well as the radiative heat loss to the ambient surrounds are neglected.
- The variation of the air temperature in the flow channel is small compared to the temperature difference $T_1 - T_{in}$. The average air temperature is T_f.
- Heat conduction inside walls is neglected.
- All walls are thermally insulated from the ambient surroundings.

In the following analysis the subscripts '1' and '2' stand for the heated wall and the unheated wall, respectively. According to the net-radiation method the radiative heat power outgoing from both the heated and the unheated wall are

$$O_{r,1} = \frac{E_1[1-(1-\varepsilon_2)\varphi_{22}] + E_2(1-\varepsilon_1)\varphi_{21}}{\Delta} \tag{A.2}$$

$$O_{r,2} = \frac{E_2[1-(1-\varepsilon_1)\varphi_{11}] + E_1(1-\varepsilon_2)\varphi_{12}}{\Delta} \tag{A.3}$$

with

$$\Delta = [1-(1-\varepsilon_1)\varphi_{11}][1-(1-\varepsilon_2)\varphi_{22}] - (1-\varepsilon_1)(1-\varepsilon_2)\varphi_{12}\varphi_{21}. \tag{A.4}$$

For the system considered the view factors are

$$\varphi_{11} = 0 \tag{A.5}$$

$$\varphi_{12} = 1 \tag{A.6}$$

$$\varphi_{21} = \frac{B}{B+2L} \tag{A.7}$$

$$\varphi_{22} = \frac{2L}{B+2L}. \tag{A.8}$$

The net radiative heat power of the heated wall is

$$Q_{r,1} = E_1 - \varepsilon_1(O_{r,1}\varphi_{11} + O_{r,2}\varphi_{21}). \tag{A.9}$$

Combining equations (A.2)–(A.9) yields

$$Q_{r,1} = \frac{\varepsilon_2 E_1 - \varepsilon_1 E_2 \dfrac{B}{B+2L}}{\varepsilon_2 + \varepsilon_1(1-\varepsilon_2)\dfrac{B}{B+2L}}. \tag{A.10}$$

The net radiative heat power of the unheated wall is equal to that of the heated wall. Therefore, the net radiative heat power of the unheated wall is obtained

$$q_{r,2} = \frac{Q_{r,1}}{(B+2L)H} = \frac{\sigma\varepsilon_1\varepsilon_2(T_1^4 - T_2^4)}{\varepsilon_2(1+2l)+\varepsilon_1(1-\varepsilon_2)} = R(T_1 - T_2) \tag{A.11}$$

with

$$R = \frac{c_T 4\sigma\varepsilon_1\varepsilon_2 T_1^3}{\varepsilon_2(1+2l)+\varepsilon_1(1-\varepsilon_2)} \tag{A.12}$$

$$c_T = \frac{1}{4}\left\{1 + \frac{T_2}{T_1} + \left(\frac{T_2}{T_1}\right)^2 + \left(\frac{T_2}{T_1}\right)^3\right\}. \tag{A.13}$$

On the unheated wall the convective heat flux is equal to the radiative heat flux:

$$q_{c,2} = h_2(T_2 - T_f) = q_{r,2} = R(T_1 - T_2). \tag{A.14}$$

This leads to the following equation:

$$q_{r,2} = \frac{Rh_2}{R+h_2}(T_1 - T_f). \tag{A.15}$$

Thus, the ratio of the radiative heat flux to the convective heat flux at the heated wall is

$$\frac{q_{r,1}}{q_{c,1}} = \frac{Q_{r,1}/B\cdot H}{h_1(T_1 - T_f)} = (1+2l)\frac{h_2}{h_1}\frac{R}{R+h_2}. \tag{A.16}$$

In case that the emissivity of all walls is the same ε, equation (A.16) is rewritten as:

$$\frac{q_{r,1}}{q_{c,1}} = (1+2l)\frac{c_T\cdot R_0/h_1}{1+c_T\cdot(h_1/h_2)\cdot(R_0/h_1)} \tag{A.17}$$

with

$$R_0 = \frac{4\sigma\varepsilon T_1^3}{2+2l-\varepsilon}. \tag{A.18}$$

The parameter c_T and h_1/h_2 depend on the temperature of both the heated wall and the unheated wall, which cannot be determined analytically. In the present study, two empirical coefficients a, b have been introduced and equation (A.17) is reduced to

$$\frac{q_{r,1}}{q_{c,1}} = (1+2l)\frac{a\cdot R_s}{1+b\cdot R_s} \tag{A.19}$$

with

$$R_s = \frac{R_0}{h_1} = \frac{1}{2+2l-\varepsilon}\cdot\frac{St}{Nu_c} \tag{A.20}$$

$$St = \frac{4\sigma\cdot\varepsilon\cdot T_1^3\cdot l_0}{\lambda} \tag{A.21}$$

$$Nu_c = \frac{h_1\cdot l_0}{\lambda}. \tag{A.22}$$

The characteristic length l_0 is the equivalent hydraulic diameter of the flow channel and is defined as:

$$l_0 = \frac{2\cdot B\cdot L}{B+L}. \tag{A.23}$$